# Band gap reduction in InN$_X$Sb$_{1-X}$ alloys: Optical absorption, k · P modeling, and density functional theory

W. M. Linhart' , M. K. Rajpalke, J. Buckeridge, P. A. E. Murgatroyd, J. J. Bomphrey, J. Alaria, C. R. A. Catlow, D. O. Scanlon, M. J. Ashwin, and T. D. Veal'

# Band gap reduction in InN$_x$Sb$_{1-x}$ alloys: Optical absorption, k · P modeling, and density functional theory

W. M. Linhart,[1,a)] M. K. Rajpalke,[2] J. Buckeridge,[3] P. A. E. Murgatroyd,[2] J. J. Bomphrey,[4] J. Alaria,[2] C. R. A. Catlow,[3] D. O. Scanlon,[3,5] M. J. Ashwin,[4] and T. D. Veal[2,b)]

[1]*Laboratory for Optical Spectroscopy of Nanostructures, Faculty of Fundamental Problems of Technology, Wrocław University of Technology, Wybrzeże Wyspiańskiego 27, Wrocław, Poland*
[2]*Stephenson Institute for Renewable Energy and Department of Physics, School of Physical Science, University of Liverpool, Liverpool L69 7ZF, United Kingdom*
[3]*University College London, Department of Chemistry, London WC1H 0AJ, United Kingdom*
[4]*Department of Chemistry, University of Warwick, Coventry CV4 7AL, United Kingdom*
[5]*Diamond Light Source Ltd., Didcot, Oxfordshire OX11 0DE, United Kingdom*

Using infrared absorption, the room temperature band gap of InSb is found to reduce from 174 (7.1 $\mu$m) to 85 meV (14.6 $\mu$m) upon incorporation of up to 1.13% N, a reduction of ~79 meV/%N. The experimentally observed band gap reduction in molecular-beam epitaxial InNSb thin films is reproduced by a five band k · P band anticrossing model incorporating a nitrogen level, $E_N$, 0.75 eV above the valence band maximum of the host InSb and an interaction coupling matrix element between the host conduction band and the N level of $\beta = 1.80$ eV. This observation is consistent with the presented results from hybrid density functional theory. © 2016 Author(s). All article content, except where otherwise noted, is licensed under a Creative Commons Attribution (CC BY) license (http://creativecommons.org/licenses/by/4.0/). [http://dx.doi.org/10.1063/1.4963836]

The substitution of highly electronegative nitrogen for a few percent of the host anions in III-V semiconductors is known to lead to a significant band gap reduction. Such dilute nitride III-V compounds have attracted attention in recent years due to realised device applications, including subcells in world record efficiency multi-junction solar cells, as in the case of GaInNAsSb,[1] and potential applications such as light sources and photodetectors in the long-wavelength infrared range.[2–4] The property of band gap reduction upon N incorporation has already been observed in GaNAs,[5] GaNP,[6] GaInNAs,[7] InNAs,[8] and GaNSb.[9,10] It has been described in terms of conduction band anticrossing (BAC), wherein a localized nitrogen level interacts with the extended host conduction band.[7] The linear combination of isolated nitrogen states model also describes this phenomenon very well.[11–14]

InSb has the smallest band gap of any common binary III–V semiconductor, having a value of 174 meV at room temperature, corresponding to a wavelength of ~7 $\mu$m. InNSb has long been proposed as an alternative to InAsSb for use in the 8–14 $\mu$m atmospheric transmission window.[15] Some evidence has been reported that the addition of N to form InNSb results in a dramatic reduction of the fundamental band gap.[2,16–18] However, several early studies were hampered by non-optimal samples in which the N content was not well known and/or hydrogen was added to stabilize an electron cyclotron resonance N plasma source.[2,16,17,19,20] In other samples, grown by radio frequency N plasma source-assisted MBE, fundamental band gap reduction in the InNSb films grown on semi-insulating GaAs was inferred from modeling of data of Burstein–Moss shifted absorption edges versus degenerate carrier concentrations.[21,22] However, quantitative modeling relied on assumed band anticrossing parameters rather than those determined from experimental results. Photoluminescence has been observed from InNSb grown by metal-organic vapor phase epitaxy, but without a clear trend of band gap versus N content.[23]

In addition to band gap reduction, the Auger recombination rate for InNSb alloys has been suggested to be three times lower than that of comparable band gap HgCdTe alloys due to the high electron effective mass, which makes InNSb a promising material for long-wavelength light sources and photodetectors.[2,24] However, in spite of continued interest in InNSb alloys over the last 15 years, straightforward optical spectroscopic evidence of the band gap reduction in samples of known N content has still not been reported and so reliable BAC parameters have not been determined.

In this letter, infrared absorption measurements of the band gap of epitaxial InNSb thin films with nitrogen incorporation of up to 1.13% are presented, analyzed using the BAC model, and compared with the results of hybrid density functional theory (DFT). The band gap of InN$_x$Sb$_{1-x}$ alloys is shown to decrease from 174 meV (7.1 $\mu$m) for $x = 0$ to 85 meV (14.6 $\mu$m) for x = 1.13%, which corresponds to a band gap reduction of ~79 meV/%N. Simulations of the absorption, based on a joint density of states method, including the BAC interaction reproduce the experimental absorption spectra well. The band gap reduction as a function of N content is also well reproduced by the BAC model. The BAC matrix element coupling strength is estimated to be 1.80 eV, using a nitrogen level of 0.75 eV above the valence band maximum (VBM). These findings and preliminary low temperature absorption measurements are consistent with the hybrid DFT results. Overall, these results indicate that InNSb alloys are suitable for sources and detectors operating in the 8–14 $\mu$m atmospheric transmission window and

a)Electronic mail: wojciech.linhart@gmail.com
b)Electronic mail: T.Veal@liverpool.ac.uk

provide the BAC parameters needed for modeling for understanding related quaternary alloys such as GaInNSb and InNSbBi and for future device design.

The InNSb epilayers were grown at the University of Warwick by N plasma assisted solid-source MBE on 100 nm InSb buffer layers on quarters of 51 mm diameter undoped InSb(001) substrates. Prior to growth, the N plasma was struck in a separate chamber with a power of 500 W and a flow rate of 0.2 sccm. The InNSb epilayers were grown to a thickness of $\sim$400 nm at a fixed growth rate of nominally 0.5 $\mu$m h$^{-1}$ using substrate temperatures, determined by pyrometer, ranging from 270 to 365 °C. The surface morphology was investigated by atomic force microscopy (AFM) with an Asylum research MFP-3D microscope in tapping mode. The lattice constant of the InNSb films was determined using high resolution X-ray diffraction (XRD) using a Philips X'Pert diffractometer equipped with monochromatic Cu K$\alpha_1$ X-ray source ($\lambda = 0.15406$ nm) with a four bounce Ge monochromator. XRD analysis was performed using the Panalytical X'pert Epitaxy application. AFM indicates the root mean square roughness values (uncorrelated with N content) in the range of 0.5–3.0 nm for all samples from $5 \times 5 \, \mu$m$^2$ images. There is no evidence from AFM measurements of any condensation of Sb on the films' surface. Transmittance measurements were performed at room temperature using a Bruker Vertex 70V Fourier-transform infrared spectrometer, using a liquid nitrogen-cooled HgCdTe detector between 50 and 1200 meV. Additionally, transmission measurements were made in the temperature range 4–300 K for a film with 0.73% N content using a continuous-flow He cryostat.

The incorporation of N in InSb has also been investigated using DFT calculations employing hybrid functionals which often provide better structural data and more accurate band gaps than the local density and generalized gradient approximations.[25–29] Here, the screened HSE06 (Heyd-Scuseria-Ernzerhof) hybrid density functional is used,[30] as implemented in the Vienna Ab initio Simulation Package (VASP).[31–33] The value of exact nonlocal exchange, $\alpha$, was 31.0%, which gives a band gap of 231 meV for InSb, in good agreement with the 0 K band gap of 235 meV extrapolated from the low temperature experimental data.[34] The valence–core interaction was described using the projector augmented wave (PAW) approach,[35] and cores of [Kr] for indium and antimony and [He] for nitrogen are used. A cutoff of 400 eV was used for all the calculations, with the Brillouin zone sampled employing a $8 \times 8 \times 8$ Monkhorst Pack grid, which provided convergence in the total energy of $10^{-4}$ eV. N incorporation was modeled by substituting one Sb for an N in a $2 \times 2 \times 2$ expansion of the 8 atom cubic cell (i.e., a 64 atom supercell), corresponding to an N concentration of 3.125%. This supercell size has been shown to be well converged when modeling N in other III–V materials.[36,37] Geometry optimisation was deemed to have converged when the forces on all the atoms were less than 0.01 eV Å$^{-1}$. The band structure of the supercell containing one N was unfolded to the primitive cell band structure using the BandUP code.[38,39] All the calculations included spin-orbit coupling, which, for bulk InSb gives a

spin-orbit valence band split off of 800 meV, in good agreement with experiment (803 meV).[40]

The N fraction was determined for epilayers grown at temperatures between 270 and 365 °C using a fixed growth rate of 0.5 $\mu$m h$^{-1}$. Both the N fraction and the epilayer thickness were determined by XRD, where both the 004 peak splitting and the Pendellösung fringes were modeled by dynamical simulations. The epilayer peak occurs at higher Bragg angle than the substrate peak, corresponding to the InNSb layer having a smaller lattice parameter than that of InSb. The N content was determined under the assumption that Vegard's law is valid using an endpoint lattice parameter for zinc blende InN of 5.01 Å.[41] Example measurements and simulations are shown in Fig. 1 for layers with 1.13 and 0.73% of their Sb sublattice substituted by N atoms. (The sample with 0.73% N was grown in a separate growth run from the others in order to fill the composition gap between 0.54% and 1.1% N. By the time of the later growth run, the N plasma source aperture plate had been modified and so, to fill the composition gap, the sample was grown at 275 °C but at a higher growth rate of 1.75 $\mu$m h$^{-1}$.) The N content from XRD (for fixed N plasma source conditions and fixed growth rate) increases as the growth temperature decreases and begins to reach a plateau corresponding to $x = 1.14$% for growth temperatures below approximately 270 °C (see Fig. S1 of supplementary material). These results are similar to those of Zhang *et al.* who grew InNSb at between 250 and 350 °C.[42] The temperature dependence of the N incorporation in InN$_x$Sb$_{1-x}$ has been modeled using the kinetic approach of Wood *et al.*[43] and Pan *et al.*,[44] which has previously been applied to N incorporation in GaNSb and GaInNSb alloys.[45,46] The curve shown in Fig. S1 is a very good fit to the experimental data and corresponds to an energy barrier for loss of N of 1.79 eV and a characteristic surface residence lifetime of N atoms of 5 $\mu$s. For comparison, the previously reported equivalent values for GaNSb are 2.0 eV and 5 $\mu$s.[45] This lower energy barrier is consistent with the
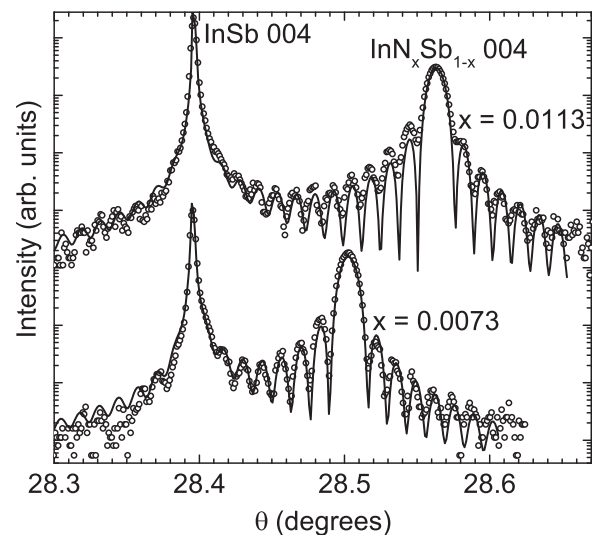


FIG. 1. XRD (points) of the 004 diffraction maximum from the InNSb films grown on an InSb substrate at 275 °C at growth rates of 0.5 and 1.75 $\mu$m h$^{-1}$. The results of the simulations (solid line) indicate that the InNSb films contain 1.13 and 0.73% N and their thickness are $390 \pm 10$ nm and $400 \pm 10$ nm, respectively.

requirement to grow InSb at a lower temperature than GaSb for N incorporation.

The band structure close to the $\Gamma$ point of $InN_xSb_{1-x}$ alloys was calculated using the **k·P** BAC model.[47–49] The dispersion of the $E_\pm$ subbands can be determined by finding the eigenvalues of the $2 \times 2$ determinant

$$\begin{vmatrix} E_c(x) - E & \beta\sqrt{x} \\ \beta\sqrt{x} & E_N(x) - E \end{vmatrix} = 0, \tag{1}$$

where $E_c(x) = E_{c0} - \alpha x$ and $E_N(x) = E_{N0} - \gamma x$ are the assumed energies of the conduction band edge and isolated N level with respect to the InSb valence band maximum (VBM). The values $\alpha = 2.44\,\text{eV}$ and $\gamma = 2.47\,\text{eV}$ are taken from fitting to previous tight binding results.[50] The $x$-dependence of the effective N level is due to interactions with other N-related states, such as different N pair and cluster configurations that are more likely to occur as the N content, $x$, increases. The value of $\beta$ is determined by fitting to the experimental data. Within this model, the host InSb conduction band and its nonparabolicity are described by Pidgeon and Brown's $(4 \times 4)$ **k·P** Hamiltonian that includes interactions of the InSb conduction band with the valence bands and the influence of higher lying bands.[51] So this results in a $(5 \times 5)$ Hamiltonian (or $(10 \times 10)$ if spin degeneracy is included) to describe the InNSb. As a result of the interaction of the nitrogen level with the host conduction band, two conduction subbands form and are denoted as $E_+$ and $E_-$. An example with $x = 1\%$ is shown in Fig. 2.

The optical properties of the InNSb epilayers as a function of N content were studied using transmission measurements. The transmission data from each sample were divided by the transmission from a different quarter of the same InSb wafer so that the remaining signal corresponds to transmission through the InNSb layer. This ratioing of the sample data with data from an InSb substrate accounts for the decrease in $\Delta\alpha$ above the band gap of the InSb—the absorption of InNSb converges to that of InSb as $E_+$ approaches the InSb conduction band (see Fig. 2). The absorption spectra calculated from the transmission data for the samples
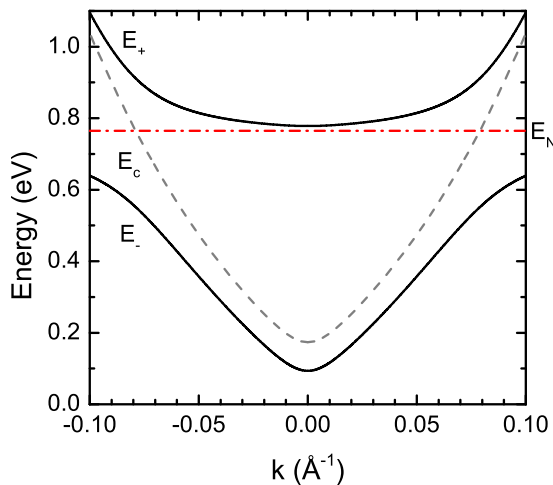
with $x = 0.54\%$, $0.73\%$, and $1.1\%$ are shown in Fig. 3(a). The band gap red shifts with increasing N content. The absorption edge decreases in energy to $85 \pm 15\,\text{meV}$ as the N content is increased to $x = 1.13\%$, corresponding to a wavelength of $\sim 14.6\,\mu m$. This corresponds to a band gap reduction of $79 \pm 5\,\text{meV}/\%N$. Model absorption curves are shown in Fig. 3(b). The approach of Perlin *et al.*[52] has been used to calculate the model absorption spectra. Accordingly, the absorption coefficient, $\alpha$, is

$$\alpha(E) \propto \sum_{c,v} \frac{|P_{cv}|^2 g_{cv}(E)}{h\nu}, \tag{2}$$

where $g_{cv}(E)$ is the joint density of states, $h\nu$ is the incident photon energy, and $P_{cv}$ are the momentum matrix elements for the optical transitions, derived from the BAC model. Here, the calculated absorption of InSb was subtracted from the calculated absorption spectrum of $InN_xSb_{1-x}$ which is equivalent to ratioing the transmission data. Within this model approach, the trends observed in the experimental absorption spectra are well reproduced. The absorption onsets are sharper in the model than the measured curves as a result of lifetime broadening being neglected.

The experimental absorption edge as a function of N content is shown by the open circles in Fig. 4. The BAC model well reproduces the trend of the band gap reduction, which is determined by the transition between the VBM and the minimum of the $E_-$ subband, which is shown by the thick solid line in Fig. 4. Within the BAC model, the adjustable parameters of the InNSb band structure are the energy of the N impurity level, $E_N$, and the BAC coupling strength, $\beta$, in the coupling matrix element, $V_{MN} = \beta\sqrt{x}$. The N level is set to 0.75 eV above the VBM, according to the results of previous tight binding calculations.[50] The optimum fit is then
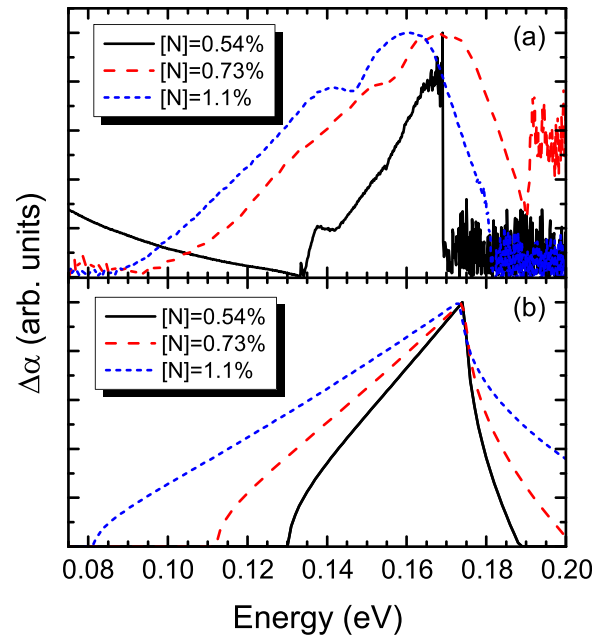


FIG. 2. (a) Conduction band dispersion of $InN_{0.01}Sb_{0.99}$ close to the $\Gamma$ point of the Brillouin zone calculated using the **k·P** BAC model. The host conduction band (dashed line) interacts with the N level (dashed-dotted line) and results in two conduction subbands $E_-$ and $E_+$ (solid lines).



FIG. 3. (a) Absorption spectra from $InN_xSb_{1-x}$ with $x = 0.54\%$ (solid line), $0.73\%$ (dashed line), and $1.1\%$ (dashed-dotted line) grown on InSb substrates. $\Delta\alpha$ denotes the difference in absorption by the InNSb film on InSb substrate and by InSb substrate alone. (b) The calculated absorption spectra within the BAC model.
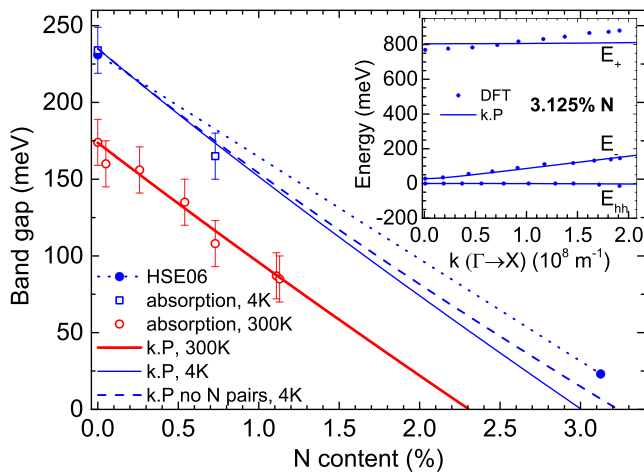
FIG. 4. The room temperature (300 K) band gap versus N content determined from the absorption spectra for the $InN_xSb_{1-x}$ samples with $0 < x \leqslant 1.13\%$ (open red circles) and calculated composition dependence of the band gap of $InN_xSb_{1-x}$ using the $\mathbf{k} \cdot \mathbf{P}$ BAC model (thick solid red line). The hybrid DFT band gaps (0 K) for InSb and InNSb with 3.125% N are also shown (closed blue circles) and joined by a dotted blue line. The 4 K experimental band gaps from optical absorption of InSb and InNSb with 0.73% N are also shown (open blue squares). The thin solid blue line is the band gap variation for 4 K using the $\mathbf{k} \cdot \mathbf{P}$ BAC model and the dashed blue line is from the same model but with a fixed effective N level, equivalent to removing the effect of N pairs and clusters. Inset is the $\Gamma$ to X direction band dispersions of the highest valence band (the heavy hole valence band) and the two lowest conduction bands (the $E_-$ and $E_+$ subbands from hybrid density functional theory (points) and the $\mathbf{k} \cdot \mathbf{P}$ modeling (solid lines).

given by adjusting the value of $\beta$ to 1.80 eV. The band gap reduction is ~79 meV/%N due to downward shift of the conduction band minimum due to the BAC interaction.

The interaction strength of $\beta = 1.80$ eV is similar to the value of 1.99 eV suggested by tight binding calculations.[50] The BAC parameters determined here differ significantly from those recommended in Vurgaftman and Meyer's review[34] where, largely based on the work by Murdin et al.[16] but using an N content-independent N level, they suggested $E_N = 0.65$ eV and $\beta = 3.0$ eV. These values correspond to 145 meV/%N band gap reduction and band gap closure for ~1.25% N at room temperature.

Results from hybrid DFT are also shown in Fig. 4 for InSb and InNSb with 3.125% N. As the DFT corresponds to 0 K, the results are compared with absorption results at 4 K for InSb and one InNSb sample with 0.73% N (see Fig. S2 of supplementary material). The DFT band gap of InNSb with 3.125% N is 23 meV. Assuming linear variation of band gap with N content, this gives a band gap reduction of 67 meV/%N. This is somewhat lower than the room temperature experimental value, which is probably due to the absence of N pair and cluster effects in DFT calculations using a 64 atom supercell containing only one N atom, which corresponds to a perfectly ordered array of substitutional N atoms, rather than a random distribution. The low temperature band gap dependence on N content has been calculated using $\mathbf{k} \cdot \mathbf{P}$ with and without the effects of N pairs and clusters on the effective N level and is shown in Fig. 4. The band gap reduction per %N, when the N level is fixed, is similar to the DFT results for N contents greater than 1.5%.

The dispersions from DFT in the $\Gamma$ to X direction for the heavy hole valence band and the lowest two conduction

bands, $E_-$ and $E_+$, are shown in inset in Fig. 4. The band dispersions from $\mathbf{k} \cdot \mathbf{P}$ calculations are also shown. Without significantly changing the band dispersions, the value of $\beta$ in the $\mathbf{k} \cdot \mathbf{P}$ was adjusted from 1.80 to 1.65 eV to reproduce the DFT band gap for $x = 3.125\%$ N. The $\mathbf{k} \cdot \mathbf{P}$ dispersions match those from hybrid DFT for the topmost valence band and the $E_-$ subband. The energy position of the $E_+$ band is similar for both methods, but with flatter dispersion in the $\mathbf{k} \cdot \mathbf{P}$ results.

The band gap reduction of 79 meV/%N represents a large proportional change due to the small band gap of InSb, but is about half the absolute band gap change per %N compared with that seen in GaNAs alloys (150 meV/%). This is a consequence of the N level lying more than 550 meV above the CBM in InNSb compared with only 250 meV for GaNAs. The InNSb band gap reduction per %N is greater than twice that observed per %Bi in InSbBi alloys (35 meV%Bi),[53] but is accompanied by much greater lattice parameter change due to the greater difference between the zinc blende InN and InSb lattice parameters compared with that of the zinc blende InBi and InSb parameters. Additionally, the InNSb calculation suggests that at room temperature band gap closure will occur for $x > 2.3\%$, giving a semimetallic band structure. Some circumstantial evidence of such band gap closure has previously been reported by Veal et al.[18] At low temperature (0 or 4 K), band gap closure is predicted to occur at or greater than 3% N.

See supplementary material for figures showing N content from XRD versus growth temperature along with kinetic modeling and also the absorption spectra recorded at 4 K from an InSb substrate and from InNSb/InSb with 0.73% N.

[1] R. Jones-Albertus, E. Becker, R. Bergner, T. Bilir, D. Derkacs, O. Fidaner, D. Jory, T. Liu, E. Lucow, P. Misra et al., in Symposium C - Compound Semiconductors: Thin-Film Photovoltaics, LEDs and Smart Energy Controls (Mater. Res. Soc. Symp. Proc., 2013), Vol. 1538, p. 161.

[2] B. N. Murdin, A. R. Adams, P. Murzyn, C. R. Pidgeon, I. V. Bradley, J.-P. R. Wells, Y. H. Matsuda, N. Miura, T. Burke, and A. D. Johnson, Appl. Phys. Lett. 81, 256 (2002).

[3] E. G. Camargo, K. Ueno, Y. Kawakami, Y. Moriyasu, K. Nagase, M. Satou, H. Endo, K. Ishibashi, and N. Kuze, Opt. Eng. 47, 014402 (2008).

[4] X. Z. Chen, D. H. Zhang, W. Liu, Y. Wang, J. H. Li, A. T. S. Wee, and A. Ramam, Electron. Lett. 46, 787 (2010).

[5] M. Weyers, M. Sato, and H. Ando, Jpn. J. Appl. Phys., Part 2 31, L853 (1992).

[6] J. N. Baillargeon, P. J. Pearah, K. Y. Cheng, G. E. Hofler, and K. C. Hsieh, J. Vac. Sci. Technol. B 10, 829 (1992).

[7] W. Shan, W. Walukiewicz, J. W. Ager, E. E. Haller, J. F. Geisz, D. J. Friedman, J. M. Olson, and S. R. Kurtz, Phys. Rev. Lett. 82, 1221 (1999).

[8] T. D. Veal, L. F. J. Piper, P. H. Jefferson, I. Mahboob, C. F. McConville, M. Merrick, T. J. C. Hosea, B. N. Murdin, and M. Hopkinson, Appl. Phys. Lett. 87, 182114 (2005).

[9]T. D. Veal, L. F. J. Piper, S. Jollands, B. R. Bennett, P. H. Jefferson, P. A. Thomas, C. F. McConville, B. N. Murdin, L. Buckle, G. W. Smith, and T. Ashley, Appl. Phys. Lett. **87**, 132101 (2005).

[10]J. J. Mudd, N. J. Kybert, W. M. Linhart, L. Buckle, T. Ashley, P. D. C. King, T. S. Jones, M. J. Ashwin, and T. D. Veal, Appl. Phys. Lett. **103**, 042110 (2013).

[11]A. Lindsay and E. P. O'Reilly, Phys. Rev. Lett. **93**, 196402 (2004).

[12]E. P. O'Reilly, A. Lindsay, P. J. Klar, A. Polimeni, and M. Capizzi, Semicond. Sci. Technol. **24**, 033001 (2009).

[13]S. Fahy, A. Lindsay, H. Ouerdane, and E. P. O'Reilly, Phys. Rev. B **74**, 035203 (2006).

[14]J. Buckeridge and S. Fahy, Phys. Rev. B **84**, 144120 (2011).

[15]A. D. Johnson, R. H. Bennett, J. Newey, G. J. Pryce, G. M. Williams, T. M. Burke, J. C. Jones, and A. M. Keir, in *Symposium OO - Infrared Applications of Semiconductors III* (Mater. Res. Soc. Symp. Proc., 1999), Vol. 607, p. 23.

[16]B. N. Murdin, M. Kamal-Saadi, A. Lindsay, E. P. O'Reilly, A. R. Adams, G. J. Nott, J. G. Crowder, C. R. Pidgeon, I. V. Bradley, J.-P. R. Wells *et al.*, Appl. Phys. Lett. **78**, 1568 (2001).

[17]T. Ashley, T. M. Burke, G. J. Pryce, A. R. Adams, A. Andreev, B. N. Murdin, and E. P. O'Reilly, Solid State Electron. **47**, 387 (2003).

[18]T. D. Veal, I. Mahboob, and C. F. McConville, Phys. Rev. Lett. **92**, 136801 (2004).

[19]T. D. Veal, I. Mahboob, C. F. McConville, T. M. Burke, and T. Ashley, Appl. Phys. Lett. **83**, 1776 (2003).

[20]T. J. C. Hosea, M. Merrick, and B. N. Murdin, Phys. Status Solidi A **202**, 1233 (2005).

[21]P. H. Jefferson, L. Buckle, D. Walker, T. D. Veal, S. Coomber, P. A. Thomas, T. Ashley, and C. F. McConville, Phys. Status Solidi RRL **1**, 104 (2007).

[22]K. P. Lim, S. F. Yoon, and H. T. Pham, J. Phys. D: Appl. Phys. **42**, 135419 (2009).

[23]Y. J. Jin, X. H. Tang, J. H. Teng, and D. H. Zhang, J. Cryst. Growth **416**, 12 (2015).

[24]K. P. Lim, S. F. Yoon, H. T. Pham, and S. Tripathy, J. Phys. D: Appl. Phys. **41**, 165301 (2008).

[25]M. Burbano, D. O. Scanlon, and G. W. Watson, J. Am. Chem. Soc. **133**, 15065 (2011).

[26]D. O. Scanlon, A. B. Kehoe, G. W. Watson, M. O. Jones, W. I. F. David, D. J. Payne, R. G. Egdell, P. P. Edwards, and A. Walsh, Phys. Rev. Lett. **107**, 246402 (2011).

[27]J. P. Allen, D. O. Scanlon, and G. W. Watson, Phys. Rev. B **81**, 161103(R) (2010).

[28]D. O. Scanlon, J. Buckeridge, C. R. A. Catlow, and G. W. Watson, J. Mater. Chem. C **2**, 3429 (2014).

[29]J. Buckeridge, D. O. Scanlon, A. Walsh, and C. R. A. Catlow, Comput. Phys. Commun. **185**, 330 (2014).

[30]A. V. Krukau, O. A. Vydrov, A. F. Izmaylov, and G. E. Scuseria, J. Chem. Phys. **125**, 224106 (2006).

[31]G. Kresse and J. Furthmüller, Phys. Rev. B **54**, 11169 (1996).

[32]G. Kresse and J. Hafner, Phys. Rev. B **47**, 558 (1993).

[33]G. Kresse and J. Furthmüller, Comput. Mater. Sci. **6**, 15 (1996).

[34]I. Vurgaftman and J. R. Meyer, J. Appl. Phys. **94**, 3675 (2003).

[35]P. E. Blöchl, Phys. Rev. B **50**, 17953 (1994).

[36]A. M. Teweldeberhan and S. Fahy, Phys. Rev. B **72**, 195203 (2005).

[37]J. Buckeridge, D. O. Scanlon, T. D. Veal, M. J. Ashwin, A. Walsh, and C. R. A. Catlow, Phys. Rev. B **89**, 014107 (2014).

[38]P. V. C. Medeiros, S. Stafström, and J. Björk, Phys. Rev. B **89**, 041407 (2014).

[39]P. V. C. Medeiros, S. S. Tsirkin, S. Stafström, and J. Björk, Phys. Rev. B **91**, 041116 (2015).

[40]M. Cardona, N. E. Christensen, and G. Fasol, Phys. Rev. B **38**, 1806 (1988).

[41]J. Schörmann, D. J. As, K. Lischka, P. Schley, R. Goldhahn, S. F. Li, W. Löffler, M. Hetterich, and H. Kalt, Appl. Phys. Lett. **89**, 261903 (2006).

[42]Y. H. Zhang, P. P. Chen, H. Yin, T. X. Li, and W. Lu, J. Phys. D: Appl. Phys. **43**, 305405 (2010).

[43]C. E. C. Wood, D. Desimone, K. Singer, and G. W. Wicks, J. Appl. Phys. **53**, 4230 (1982).

[44]Z. Pan, L. H. Li, W. Zhang, Y. W. Lin, and R. H. Wu, Appl. Phys. Lett. **77**, 214 (2000).

[45]M. J. Ashwin, T. D. Veal, J. J. Bomphrey, I. R. Dunn, D. Walker, P. A. Thomas, and T. S. Jones, AIP Adv. **1**, 032159 (2011).

[46]M. J. Ashwin, D. Walker, P. A. Thomas, T. S. Jones, and T. D. Veal, J. Appl. Phys. **113**, 033502 (2013).

[47]J. Wu, W. Shan, and W. Walukiewicz, Semicond. Sci. Technol. **17**, 860 (2002).

[48]A. Lindsay and E. O'Reilly, Solid State Commun. **112**, 443 (1999).

[49]E. P. O'Reilly, A. Lindsay, and S. Fahy, J. Phys.: Condens. Matter **16**, S3257 (2004).

[50]A. Lindsay, E. P. O'Reilly, A. D. Andreev, and T. Ashley, Phys. Rev. B **77**, 165205 (2008).

[51]C. R. Pidgeon and R. N. Brown, Phys. Rev. **146**, 575 (1966).

[52]P. Perlin, P. Winiewski, C. Skierbiszewski, T. Suski, E. Kamiska, S. G. Subramanya, E. R. Weber, D. E. Mars, and W. Walukiewicz, Appl. Phys. Lett. **76**, 1279 (2000).

[53]M. K. Rajpalke, W. M. Linhart, K. M. Yu, M. Birkett, J. Alaria, J. J. Bomphrey, S. Sallis, L. F. J. Piper, T. S. Jones, M. J. Ashwin, and T. D. Veal, Appl. Phys. Lett. **105**, 212101 (2014).